J|A|C|S
ARTICLES
Published on Web 03/23/2002

Mechanistic Comparison of Cyclic Ester Polymerizations by Novel Iron(III)−Alkoxide Complexes: Single vs Multiple Site Catalysis

Brendan J. O'Keefe, Laurie E. Breyfogle, Marc A. Hillmyer,* and William B. Tolman*

Contribution from the Department of Chemistry, University of Minnesota, 207 Pleasant Street SE, Minneapolis, Minnesota 55455

Received December 12, 2001

Abstract: The complexes $Fe_2(OCHPh_2)_6$ and L_2FeOR (R = Et or $CHPh_2$, L = *N*,*N*′-bis(trimethylsilyl)-benzamidinate) were structurally characterized, and comparative studies of the behavior of those compounds comprising the same alkoxide (Ph_2HCO^-) in polymerizations of ϵ-caprolactone (CL) and D,L-lactide (LA) were performed. Both $Fe_2(OCHPh_2)_6$ and $L_2FeOCHPh_2$ are effective polymerization catalysts, as reflected by molecular weight control, polydispersities, and end group analysis, but the diiron complex generally exhibits greater polymerization control, particularly for CL. Kinetic investigations of the polymerization of CL revealed the same first-order dependence on [CL] for both catalysts, but different orders in [catalyst] that signified a distinct contrast in mechanism. Analysis that invoked the presence of a termination-causing impurity at low concentration yielded a first-order dependence on $[Fe_2(OCHPh_2)_6]$, but the order in $[L_2FeOCHPh_2]$ was found to be one-half. This fractional dependence was interpreted by using a model of active chain aggregation. Comparison of the derived propagation rate constants (k_{prop}) revealed a ~50-fold greater value for the diiron complex compared to the single site mononuclear compound. Implications of these findings for understanding cyclic ester polymerization mechanisms and catalyst design are discussed.

Introduction

The ring-opening polymerization of cyclic esters with metal complexes as catalysts enables the convenient and efficient preparation of a range of polyesters, such as polylactides and polylactones.[1] These plastics are of great interest due to their utility in numerous applications,[2] the renewable nature of some of their cyclic ester precursors (e.g., lactide from corn), and their biodegradable characteristics, all of which provide a basis for the development of new sustainable commercial technologies.[2,3] Many types of metal alkoxides have been found to be active cyclic ester polymerization catalysts, and in many cases yield materials with prescribed molecular weights and narrow molecular weight distributions. Understanding the relationship between the structural features of metal−alkoxide complexes and their polymerization efficiency, selectivity, and mechanism is an important aim of current research.[1]

The known active metal−alkoxide catalytic precursors generally may be divided into two classes according to their structural type. One set includes homoleptic complexes $M_x(OR)_y$ and related oxo-containing clusters which are typically multinuclear ($x \geq 1$) and contain multiple alkoxides ($y > 2$). Examples include $Ln_5(O)(OR)_{13}$ (Ln = lanthanide(III) or yttrium(III) ion),[4] species derived from $Y(OAr)_3$ (OAr = phenoxide) and alcohols,[5] "$Y(OCH_2CH_2NMe_2)_3$",[6] $Al(OiPr)_3$,[7] and $Sn(OR)_2$,[8] which typically aggregate in solution. Members of the second class are of the type $L_zM_x(OR)_y$, where L denotes an ancillary supporting ligand that often results in lower nuclearity species (e.g., $x = 1$) with fewer alkoxides ($y \leq 2$; for a catalog of examples, see ref 1a). Polymerization initiation and propagation for both classes is believed to proceed via a coordination−insertion mechanism, in which a metal−alkoxide attacks the cyclic ester carbonyl carbon, the ring opens, and a new metal alkoxide is formed.[9] Mechanistic complexity may arise for the $M_x(OR)_y$ complexes because of their multiple iniation sites and their propensity to participate in aggregation equilibria in solution.[7] Complexes of the $L_zM_x(OR)_y$ type have been targeted partly in order to address these potential deficiencies, a key objective

* To whom correspondence should be addressed. E-mail: hillmyer@chem.umn.edu, tolman@chem.umn.edu.

(1) (a) O'Keefe, B. J.; Hillmyer, M. A.; Tolman, W. B. *J. Chem. Soc., Dalton Trans.* **2001**, 2215−2224. (b) Kuran, W. *Prog. Polym. Sci.* **1998**, *23*, 919−992. (c) Löfgren, A.; Albertsson, A.-C.; Dubois, P.; Jérôme, R. *J. Macromol. Sci., Rev. Macromol. Chem. Phys.* **1995**, *C35*, 379−418.

(2) (a) Amass, W.; Amass, A.; Tighe, B. *Polym. Int.* **1998**, *47*, 89−144. (b) Drumwright, R. W.; Gruber, P. R.; Henton, D. E. *Adv. Mater.* **2000**, *12*, 1841−1846. (c) Ikada, Y.; Tsuji, H. *Macromol. Rapid Commun.* **2000**, *21*, 117−132.

(3) Tullo, A. *Chem. Eng. News* **2000**, *78* (no. 3, January 17), p 13. Also see: http://www.cargilldow.com.

(4) Simic, V.; Spassky, N.; Hubert-Pfalzgraf, L. G. *Macromolecules* **1997**, *30*, 7338−7340 and references therein.

(5) (a) Stevels, W. M.; Ankoné, M. J. K.; Dijkstra, P. J.; Feijen, J. *Macromolecules* **1996**, *29*, 3332−3333. (b) Stevels, W. M.; Ankone, M. J. K.; Dijkstra, P. J.; Feijen, J. *Macromolecules* **1996**, *29*, 6132−6138.

(6) McLain, S. J.; Drysdale, N. E. *Polym. Prepr. (Am. Chem. Soc., Div. Polym. Chem.)* **1992**, *33*, 174 and 463.

(7) Kowalski, A.; Duda, A.; Penczek, S. *Macromolecules* **1998**, *31*, 2114−2122 and references therein.

(8) Kowalski, A.; Libiszowski, J.; Duda, A.; Penczek, S. *Macromolecules* **2000**, *33*, 1964−1971.

(9) For example, see: (a) Dubois, P.; Jacobs, C.; Jérôme, R.; Teyssié, P. *Macromolecules* **1991**, *24*, 2266−2270. (b) Kricheldorf, H. R.; Kreiser-Saunders, I. *Macromol. Symp.* **1996**, *103*, 85−102.

10.1021/ja012689t CCC: $22.00

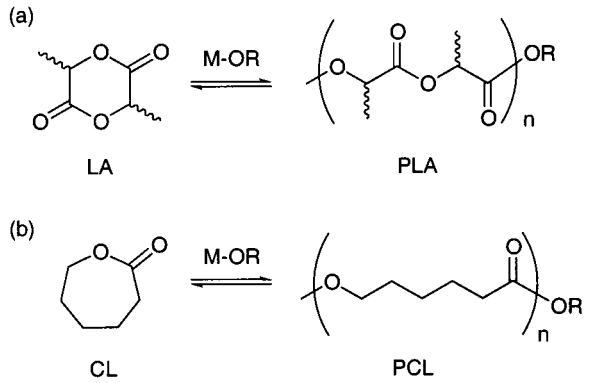

Figure 1. Metal-alkoxide promoted polymerization of (a) LA to PLA and (b) CL to PCL.

being to prepare "single site" catalysts that might exhibit simple kinetic behavior (e.g., first-order dependence on the concentration of the complex) and that may be tuned through supporting ligand manipulations.[1] Direct comparison of the polymerization behavior of such a single site system with a multisite analogue, containing the same metal ion(s) and alkoxides, would provide mechanistic insights of value for future catalyst design.

We recently reported the controlled polymerization of D,L-lactide (LA) by the novel iron(III)−alkoxide complexes $Fe_5(O)(OEt)_{13}$ and $Fe_2(OCMe_2Ph)_6$.[10] These compounds were targeted because of the low toxicity of iron(III), the presence of which is inevitable in the final polymers which may have biomedical end uses. Importantly, the complexes showed superior polymerization activity relative to previously reported iron-containing catalyst precursors.[11] Thus inspired, we turned our attention toward designing a mononuclear complex L_xFeOR with which to perform comparative mechanistic studies. Here we report the synthesis and full characterization of rare[12] examples of well-defined complexes of this type, L_2FeOR (L = *N*,*N*′-bis(trimethylsilyl)benzamidinate,[13] R = Et and $CHPh_2$), as well as a homoleptic dinuclear analogue with one of the same alkoxides, $Fe_2(OCHPh_2)_6$. Direct comparison of the reactivity of the compounds that contain the same Ph_2HCO^- initiators in the polymerization of LA and ϵ-caprolactone (CL) (Figure 1) revealed unexpected differences in kinetic behavior that raise issues of importance for the design of new cyclic ester polymerization catalysts.

Scheme 1

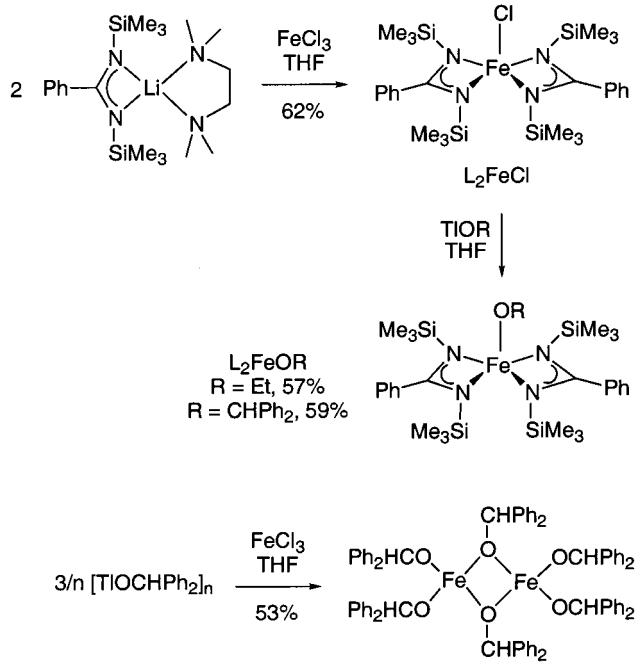

Results

Synthesis of Iron(III)−Alkoxide Complexes. The mononuclear iron(III)−alkoxide complexes L_2FeOR (R = Et or $CHPh_2$) were prepared as outlined in Scheme 1. We prepared the known intermediate complex L_2FeCl by the reaction of 2 equiv of L·Li(TMEDA)[14] with anhydrous $FeCl_3$ in THF, a route we found to be more convenient than that reported previously.[15] Elemental analysis, IR spectroscopy, and a unit cell determination of a single crystal by X-ray crystallography confirmed the identity of the product. Because of difficulties we encountered in attempts to prepare iron(III)−alkoxide complexes via metathesis reactions of L_2FeCl with sodium or lithium alkoxides, we used the thallium reagents $[TlOR]_n$ obtained commercially (R = Et) or via the precedented reaction of $[TlOEt]_n$ with benzhydrol.[16] The product of the latter reaction, $[Tl(OCHPh_2)]_n$, was isolated as a white crystalline solid, characterized by ^1H and ^{13}C NMR and IR spectroscopy, and used without further purification. Reaction of L_2FeCl and the appropriate thallium alkoxide in THF yielded the mononuclear ferric alkoxides $L_2Fe(OR)$ as dark red crystalline solids. The complexes were characterized by elemental analysis, FTIR and UV−vis spectroscopy, room temperature magnetic susceptibility in solution (Evans method, d_6-benzene),[17] and X-ray crystallography. Their red color derives from an apparent charge-transfer transition at λ_{max} = 395 nm ($\epsilon \sim 2500\ M^{-1}\ cm^{-1}$). Solution magnetic moments (μ_{eff}) of ~5.8 μ_B for both complexes are consistent with the presence of high-spin iron(III) ($S = {}^5/_2$). While we cannot be certain on the basis of the available data that the complexes are monomeric in solution, the X-ray crystal structural data confirmed their mononuclear formulations in the solid state (see below).

(10) O'Keefe, B. J.; Monnier, S. M.; Hillmyer, M. A.; Tolman, W. B. *J. Am. Chem. Soc.* **2001**, *123*, 339−340.
(11) For example, see: Stolt, M.; Södergård, A. *Macromolecules* **1999**, *32*, 6412−6417.
(12) A search of the Cambridge Crystallographic Database (version 5.21, April 2001) revealed the following reports of structurally defined mononuclear iron(III)−alkoxide complexes: (a) Prevot, L.; Jaquinod, L.; Fischer, J.; Weiss, R. *Inorg. Chim. Acta* **1998**, *283*, 98. (b) Roelfes, G.; Lubben, M.; Chen, K.; Ho, R. Y. N.; Meetsma, A.; Genseberger, S.; Hermant, R. M.; Hage, R.; Mandal, S. K.; Young, V. G., Jr.; Zang, Y.; Kooijman, H.; Spek, A. L.; Que, L., Jr.; Feringa, B. L. *Inorg. Chem.* **1999**, *38*, 1929. (c) Bochmann, M.; Wilkinson, G.; Young, G. B.; Hursthouse, M. B.; Malik, K. M. A. *J. Chem. Soc., Dalton Trans.* **1980**, 1863. (d) Lecomte, C.; Chadwick, D. L.; Coppens, P.; Stevens, E. D. *Inorg. Chem.* **1983**, *22*, 2982. (e) Johnson, M. R.; Seok, W. K.; Ma, W.; Slebodnick, C.; Wilcoxen, K. M.; Ibers, J. A. *J. Org. Chem.* **1996**, *61*, 3298. (f) Potz, R.; Huckstadt, H.; Homborg, H. *Z. Anorg. Allg. Chem.* **1998**, *624*, 173. (g) Jonas, R. T.; Stack, T. D. P. *J. Am. Chem. Soc.* **1997**, *119*, 8566−8567. (h) Hatano, K.; Uno, T. *Bull. Chem. Soc. Jpn.* **1990**, *63*, 1825.
(13) Reviews on amidinate chemistry: (a) Barker, J.; Kilner, M. *Coord. Chem. Rev.* **1994**, *133*, 219−300. (b) Edelmann, F. T. *Coord. Chem. Rev.* **1994**, *137*, 403−481. Selected more recent applications of L in Y(III) and Fe(II) chemistry: (c) Brussee, E. A. C.; Meetsma, A.; Hessen, B.; Teuben, H. H. *Chem. Commun.* **2000**, *6*, 497−498. (d) Vendemiati, B.; Prini, G.; Meetsma, A.; Hessen, B.; Teuben, J. H.; Traverso, O. *Eur. J. Inorg. Chem.* **2001**, 707−711.
(14) Dick, D. G.; Duchateau, R.; Edema, J. J. H.; Gambarotta, S. *Inorg. Chem.* **1993**, *32*, 1959−1962.
(15) Zinn, A.; von Arnim, H.; Massa, W.; Schäfer, M.; Pebler, J.; Dehnicke, K. *Z. Z. Naturforsch.* **1991**, *46b*, 1300−1304.
(16) Zechmann, C. A.; Boyle, T. J.; Pedrotty, D. M.; Alam, T. M.; Lang, D. P.; Scott, B. L. *Inorg. Chem.* **2001**, *40*, 2177−2184.
(17) Schubert, E. M. *J. Chem. Educ.* **1992**, *69*, 62.

Table 1. Summary of X-ray Crystallographic Data

	$Fe_2(OCHPh_2)_6 \cdot 2C_7H_8$	L_2FeOEt	$L_2FeOCHPh_2$
empirical formula	$C_{92}H_{82}O_6Fe_2$	$C_{28}H_{51}N_4OSi_4Fe$	$C_{39}H_{57}N_4OSi_4Fe$
formula weight	697.64	627.94	766.10
crystal system	triclinic	orthorhombic	monoclinic
space group	$P\bar{1}$	*Pbca*	$P2_1/n$
a (Å)	10.8678 (10)	18.599 (3)	19.200 (3)
b (Å)	13.5829 (12)	18.661 (3)	10.9732 (15)
c (Å)	13.7118 (12)	21.015 (3)	21.207 (3)
α (deg)	72.6420 (10)	90	90
β (deg)	78.123 (2)	90	103.074 (2)
γ (deg)	73.1550 (10)	90	90
V (Å^3)	1833.2 (3)	7294.0 (17)	4352.1 (10)
Z	1	8	4
density (calcd) (g/cm^3)	1.264	1.144	1.169
crystal color	yellow	red	red
crystal size (mm)	0.50 × 0.11 × 0.06	0.50 × 0.45 × 0.30	0.45 × 0.4 × 0.3
absorption coefficient (mm^{-1})	0.452	0.570	0.489
$2\theta_{max}$ (deg)	50.02	50.06	50.08
no. of reflcns collected	13288	51261	42909
no. of ind reflcns	6398	6444	7691
no. of obsd reflcns [$I > 2\sigma(I)$]	5496	3875	6415
parameters	470	353	442
$R1^a$ [$I > 2\sigma(I)$]	0.0521	0.0717	0.0291
$wR2^b$	0.1392	0.1344	0.0802
goodness-of-fit	1.063	1.040	1.042
largest diff peak and hole (eÅ^{-3})	1.836, −0.392	0.610, −0.259	0.267, −0.198

[a] $R1 = \sum||F_o| - |F_c||/\sum|F_o|$. [b] $wR2 = [\sum[w(F_o^2 - F_c^2)^2]/[\sum[w(F_o^2)^2]]^{1/2}$, where $w = 1/\sigma^2(F_o^2) + (aP)^2 + bP$.

Table 2. Selected Interatomic Distances (Å) and Angles (deg)[a]

	$Fe_2(OCHPh_2)_6 \cdot 2C_7H_8$		
Fe1−O1	1.799(2)	Fe1−O15	1.784(2)
Fe1−O29	1.952(2)	Fe1−O29A	1.956(2)
Fe1···Fe1A	2.955(1)		
O29−Fe1−O29A	81.76(8)	Fe1−O29−Fe1A	98.24(8)
	L_2FeOEt		
Fe1−O1	1.802(3)	Fe1−N1	2.134(3)
Fe1−N2	2.074(3)	Fe1−N3	2.062(3)
Fe1−N4	2.132(3)		
N1−Fe1−N2	65.42(14)	N3−Fe1−N4	64.97(13)
	$L_2FeOCHPh_2$		
Fe1−O1	1.842(1)	Fe1−N1	2.069(1)
Fe1−N2	2.106(1)	Fe1−N3	2.149(1)
Fe1−N4	2.046(1)		
N1−Fe1−N2	65.06(6)	N3−Fe1−N4	64.94(05)

[a] Estimated standard deviations in parentheses.

Reaction of anhydrous $FeCl_3$ with 3/*n* equiv of $[Tl(OCHPh_2)]_n$ in THF provided the dinuclear complex $Fe_2(OCHPh_2)_6$ as a yellow solid upon crystallization. The complex was characterized by elemental analysis, FTIR spectroscopy, and X-ray crystallography (see below), which confirmed its formulation as a diiron(III,III) species analogous to $Fe_2(OCMe_2Ph)_6$ that we reported previously.[10] The clean isolation of these homoleptic diiron−alkoxide complexes with thallium alkoxide reagents contrasts with the formation of higher order oxo-bridged clusters when sodium alkoxides are used.[10,18]

X-ray Crystal Structures. Crystallographic data for L_2FeOR (R = Et or $CHPh_2$) and $Fe_2(OCHPh_2)_6$ are listed in Table 1, selected interatomic distances and angles are provided in Table 2, and representations of the structures are shown in Figure 2. The two mononuclear complexes have similar structures, much like the previously described topology of L_2FeCl.[15] Each has a pentacoordinate Fe(III) ion in a geometry distorted between square pyramidal and trigonal bipyramidal, with two chelating amidinate ligands and a terminal alkoxide comprising the coordination sphere.[19] Asymmetric bonding of the amidinates to the iron atom is another common feature (e.g., Fe1−N1/N4 = 2.13 Å and Fe−N2/N3 = 2.07 Å for L_2FeOEt). The iron−oxygen (Fe1−O1) bond distances are 1.802(3) (R = Et) and 1.8417(12) Å (R = $CHPh_2$), which fall in the middle of the range reported for other mononuclear iron(III)−alkoxides (1.77−1.89 Å).[12] The Fe−O−C angles are 141.5(7)° (R = Et) and 127.6(1)° (R = $CHPh_2$), consistent with the absence of multiple Fe−OR bonding that has been identified in some complexes with more Lewis acidic Fe(III) ions supported by neutral N-donors.[12b,g]

In $Fe_2(OCHPh_2)_6$, two distorted tetrahedral Fe(III) centers are bridged by two alkoxide ligands, with two terminal alkoxides ligated to each iron atom. The geometry of the complex is similar to that of $Fe_2(OCMe_2Ph)_6$, although there are some notable differences. Both are unusual examples of doubly alkoxide bridged diiron(III,III) complexes comprising 4-coordinate metal sites.[20] Consistent with their low coordination numbers, the Fe−Fe distances in $Fe_2(OCHPh_2)_6$ and $Fe_2(OCMe_2Ph)_6$ are short (2.955(1) and 3.003(1) Å, respectively) relative to the average Fe−Fe separation of 3.16(8) Å in other known complexes with two bridging alkoxides. Finally, the terminal Fe−OR groups for the complex with R = $CHPh_2$ exhibit bent geometries with similar Fe−O distances. In contrast, one of the terminal units in $Fe_2(OCMe_2Ph)_6$ is linear (Fe1−O11−C12 = 179.69(15)°) with a short Fe−O distance (1.7631(14) Å), suggestive of multiple Fe−O bond character, while the other is bent (Fe1−O1−C2 = 137.54(12)°) with a longer Fe−O bond (1.8098(13) Å). These crystalline phase structural differences

(18) Veith, M.; Grätz, F.; Huch, V. *Eur. J. Inorg. Chem.* **2001**, 367−368.

(19) For L_2FeOEt $\tau = 0.64$ and for $L_2FeOCHPh_2$ $\tau = 0.62$. For five-coordinate complexes the τ value is a measure of the distortion of the geometry from square pyramidal ($\tau = 0$) and trigonal bipyramidal ($\tau = 1$). Addison, A. W.; Rao, T. N.; Reedijk, J.; van Rijn, J.; Verschoor, G. C. *J. Chem. Soc., Dalton Trans.* **1984**, 1349−1356.

(20) A search of the CSD (April 2001, version 5.21) gave 104 hits for complexes containing two irons and two bridging alkoxides. A manual search of these compounds revealed 60 diiron(III,III) complexes, with an average Fe−Fe separation of 3.16(8) Å.

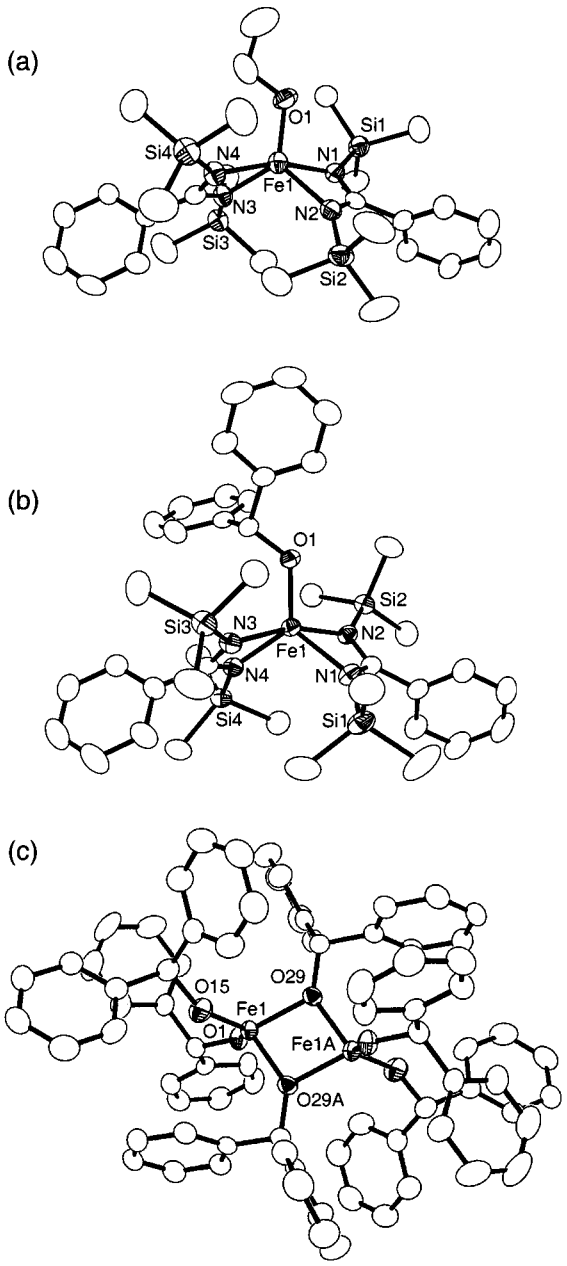

Figure 2. Representations of the X-ray crystal structures of (a) L_2FeOEt, (b) $L_2FeOCHPh_2$, and (c) $Fe_2(OCHPh_2)_6$. All atoms are shown as 50% thermal ellipsoids, with solvent and hydrogen atoms omitted for clarity.

between the analogous complexes imply that steric differences between their alkoxides are significant; the possible functional importance of these differences is a subject for further study.

Polymerization Activity. Both $Fe_2(OCHPh_2)_6$ and $L_2FeOCHPh_2$ are effective catalysts for the polymerization of CL and LA; L_2FeOEt also was effective, but we did not examine it in detail in order to focus on comparing the catalysts with identical alkoxides. Polymerizations were performed in toluene solution, at an initial monomer concentration of 1 M, at 25 °C for CL, but at 70 °C for LA due to the lack of solubility of monomer and polymer at lower temperatures. For the polymerizations of CL by both catalysts (Table 3), rapid reactions with good control of polymer molecular weight were observed over a range of monomer-to-catalyst ratios, as shown by the linear nature of plots of M_n versus conversion (Figure 3) and M_n versus the ratio of monomer conversion to initial catalyst concentration

Table 3. Selected Data for the Polymerization of CL[a]

catalyst	$[CL]_0/[Fe]_0$	time (min)	M_n (kg/mol)[b]	PDI[b]
$Fe_2(OCHPh_2)_6$	50	20	7.5	1.19
	200	26	20.9	1.20
	250	25	25.6	1.20
	300	35	28.4	1.19
	350	73	30.9	1.20
	450	960	36.4	1.20
$L_2FeOCHPh_2$	100	190	18.6	1.81
	200	255	23.1	1.82
	300	360	26.1	1.87
	400	960	27.0	1.98

[a] Conditions: $[CL]_0 = 1$ M, toluene or d_8-toluene, 25 °C. All conversions are 100%. [b] Determined by SEC vs polystyrene standards.

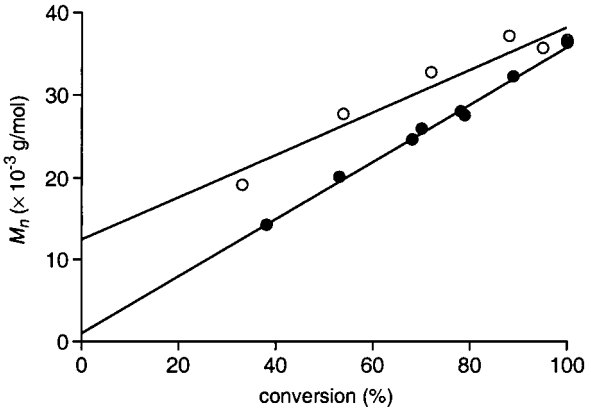

Figure 3. Plot of M_n (vs polystyrene standards) vs conversion (^{1}H NMR) for the polymerization of CL by $Fe_2(OCHPh_2)_6$ (●) and $L_2FeOCHPh_2$ (○). Conditions: $[CL]_0 = 1.0$ M, toluene, 25 °C, $[CL]_0/[Fe]_0 = 450$ for $Fe_2(OCHPh_2)_6$ or 200 for $L_2FeOCHPh_2$. Each data point represents a separate reaction.

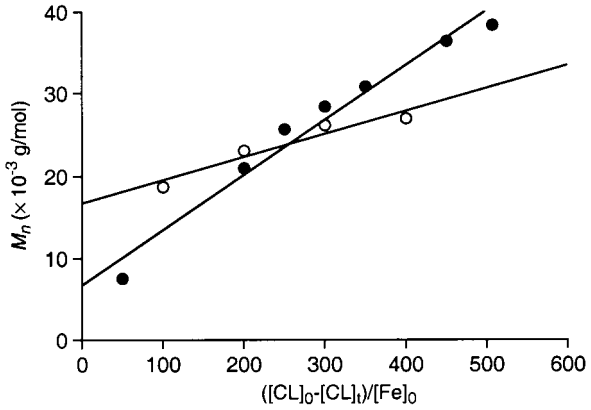

Figure 4. Dependence of M_n (vs polystyrene standards) on $([CL]_0 - [CL]_t)/[Fe]_0$ for the polymerization of CL by $Fe_2(OCHPh_2)_6$ (●) and $L_2FeOCHPh_2$ (○). Conditions: $[CL]_0 = 1.0$ M, toluene, 25 °C.

(Figure 4). Narrow molecular weight distributions (polydispersity index (PDI) ≤ 1.2) were obtained with $Fe_2(OCHPh_2)_6$ as catalyst (Table 3). Samples of PCL prepared with $L_2FeOCHPh_2$ exhibited broader molecular weight distributions, with PDI values ranging between 1.4 and 2.0. In addition, with this catalyst, we observed particularly high *y* intercepts for the lines fit to the data in Figures 3 and 4. Possible explanations for this behavior include (a) a tendency for this catalyst to engage in intramolecular transesterification reactions (yielding cyclic oligomers and, thus, lower M_n at the higher $[CL]_0 - [Cl]_t/[Fe]_0$ ratios), (b) low initiation efficiency, and/or (c) a sensitivity of the catalytic species to small amounts of impurities in the

Table 4. Selected Data for the Polymerization of LA[a]

catalyst	time (min)	conversion (%)[b]	M_n (kg/mol)[c]	PDI[c]
$Fe_2(OCHPh_2)_6$	11	37	19.3	1.09
	21	73	44.8	1.11
	27	84	45.5	1.19
	32	89	47.7	1.19
	37	94	54.4	1.25
	52	96	61.2	1.34
	6	35	14.8	1.13
	10	70	22.9	1.44
	14	93	49.0	1.26
	18	95	54.6	1.31
	34	95	55.6	1.60
$L_2Fe(OCHPh_2)$	11	33	31.8	1.34
	19	39	25.4	1.49
	30	40	43.0	1.67
	40	68	44.2	1.90
	48	68	34.7	1.86
	77	88	39.5	1.88

[a] Conditions: $[LA]_0 = 1$ M, $[LA]_0/[Fe]_0 = 1000:1$, toluene, 70 °C. [b] Determined by ^{1}H NMR. [c] Determined by SEC.

monomer that promote chain transfer. These issues are discussed further below.

The polymerization of LA (toluene, 70 °C) with $Fe_2(OCHPh_2)_6$ and $L_2FeOCHPh_2$ also proceeded rapidly. For example, for the dinuclear catalyst at $[LA]_0/[Fe]_0 = 1000:1$ a conversion of 96% was reached in 52 min to yield polymer with $M_n = 61.2 \times 10^3$ g/mol. However, the observed level of molecular weight control, polydispersity indices, and degree of reproducibility between replicate runs (Table 4) were generally poorer than for the polymerizations of CL. Thus, while PLA M_n generally increased with conversion, significant scatter from linearity in a plot of M_n vs conversion was observed, particularly when $L_2FeOCHPh_2$ was used (Figure S1). We observed relatively narrow molecular weight distributions for the PLA samples isolated at low conversions that were similar to those measured for PCL prepared using the same catalyst, but the PLA distributions broadened significantly at higher conversions (Table 4). Finally, analysis by ^{1}H NMR spectroscopy showed that PLA samples prepared from D,L-LA with $Fe_2(OCHPh_2)_6$ or $L_2FeOCHPh_2$ were atactic, indicating that there was no discernible stereocontrol in the polymerizations.[21]

In a test for a coordination−insertion polymerization mechanism, we determined the nature of the polymer end group in low molecular weight PLA and PCL samples prepared by using $[M]_0/[Fe]_0$ ratios ranging between 30 and 50 (M = CL or LA, Fe = iron sites) by ^{1}H NMR spectroscopy. For both complexes, these experiments indicated the presence of a diphenylmethoxide unit as an alkoxy ester end group, confirming that initiation (and presumably polymerization) proceeds by insertion of a monomer unit into the iron−alkoxide bond, with cleavage of the acyl−oxygen bond of the monomer. Careful integration of the end group and polymer methylene resonances enabled calculation of chain lengths, which are determined by the $[M]_0/[Fe]_0$ ratio and the number of initiating alkoxides per Fe atom. For $Fe_2(OCHPh_2)_6$ at $[M]_0/[Fe]_0 = 50:1$, if every alkoxide group initiated the polymerization of one chain the expected chain length would be 16 monomer units for PLA and 17 for PCL.[22] The NMR integration data for samples prepared with $Fe_2(OCHPh_2)_6$ gave chain lengths of 15(2) units for PLA and 25(4) for PCL, in rough agreement with the expected values. Thus, approximately every alkoxide initiates a polymer chain (≈3 initiators per Fe atom). Similar experiments were performed with $L_2FeOCHPh_2$ and CL. At $[CL]_0/[Fe]_0 = 30:1$ the expected chain length is 30, but the measured values were 68(5), indicating that only about one-half of the total possible initiators were effective. Thus, initiation by the $L_2FeOCHPh_2$ is inefficient compared to that by $Fe_2(OCHPh_2)_6$ for CL polymerization.

In further support of controlled behavior in polymerizations with $Fe_2(OCHPh_2)_6$, a PCL/PLA block copolymer was prepared via sequential reactions with the different monomers. First, a low molecular weight block of PCL was prepared ($[CL]_0/[Fe]_0 = 50:1$, 25 °C, toluene, 20 min, $M_n = 7.45 \times 10^3$ g/mol, PDI = 1.19, Figure S2a). Then 400 equiv of LA was added, and the reaction mixture was heated at 70 °C for 50 min to give the final PCL/PLA block copolymer ($M_n = 30.5 \times 10^3$ g/mol, PDI = 1.54).[23] Importantly, there was little low molecular weight polymer observed in the SEC trace of the final copolymer sample (Figure S2b), indicating that the PCL chains remained active to initiate the polymerization of LA. Integration of the ^{1}H NMR spectrum of the block copolymer gave a PLA:PCL ratio of 8.7, close to the expected ratio of 8.

Kinetics of CL Polymerizations. To best draw mechanistic comparisons between $Fe_2(OCHPh_2)_6$ and $L_2FeOCHPh_2$, we chose to investigate the kinetics of CL polymerization by these catalysts in toluene at 25 °C. The decision to study the kinetics of the polymerization of CL instead of LA was based on the higher degree of molecular weight control observed in polymerizations of CL, practical concerns that included the high solubility of CL in toluene at low temperature (thus eliminating any chance of loss of initial rate data during the warming/monomer dissolution phase of LA reactions), and the larger equilibrium constant for CL polymerization that simplified data analysis. We initially used ^{1}H NMR spectroscopy to monitor conversions in reactions using $Fe_2(OCHPh_2)_6$ (d_8-toluene) and then used in situ FTIR spectroscopy (ReactIR) for reactions using $L_2FeOCHPh_2$. The FTIR method is particularly advantageous for monitoring reactions in which high concentrations of paramagnetic catalyst are used.[24] A representative stack plot of FTIR spectra during the course of a kinetic run is shown in Figure S3; the protocol used to analyze such data is described in the Experimental Section. All reactions were run at a fixed initial monomer concentration ($[CL]_0 = 1.0$ M) while the catalyst concentration was varied over convenient ranges ($[Fe_2(OCHPh_2)_6]_0 = 9.1 \times 10^{-4}$ to 2.5×10^{-3} M; $[L_2FeOCHPh_2]_0 = 3.3 \times 10^{-3}$ to 3.3×10^{-2} M). Over the concentration ranges studied all polymerizations showed first-order dependencies on the concentration of CL over at least four half-lives. The apparent rate constant (k_{app}) for each run was obtained from the slope of the best-fit line to the plot of $\ln([CL]_0/[CL]_t)$ versus time (NMR data, Figure 5a) or, equiva-

(21) Chamberlain, B. M.; Cheng, M.; Moore, D. R.; Ovitt, T. M.; Lobkovsky, E. B.; Coates, G. W. *J. Am. Chem. Soc.* **2001**, *123*, 3229−3238.

(22) The expected chain length is lower for PLA than PCL because the equilibrium conversion for LA polymerization ($[LA]_0 = 1$ M) is ~96% at 70 °C in toluene, while it is ~100% for CL polymerization at 25 °C in toluene. For the equilibrium monomer concentration of LA in toluene see: Wang, Y.; Hillmyer, M. A. *Macromolecules* **2000**, *33*, 7395−7403.

(23) We lack precise knowledge of the copolymer architecture, so we cannot rule out transesterification and resulting formation of structures more complex than a simple AB diblock.

(24) In a confirmation that the observed rate constants were not dependent on the monitoring technique, several runs with $Fe_2(OCHPh_2)_6$ were followed by FTIR spectroscopy and were found to yield rate constants that were identical within experimental error to those determined by using the NMR method.

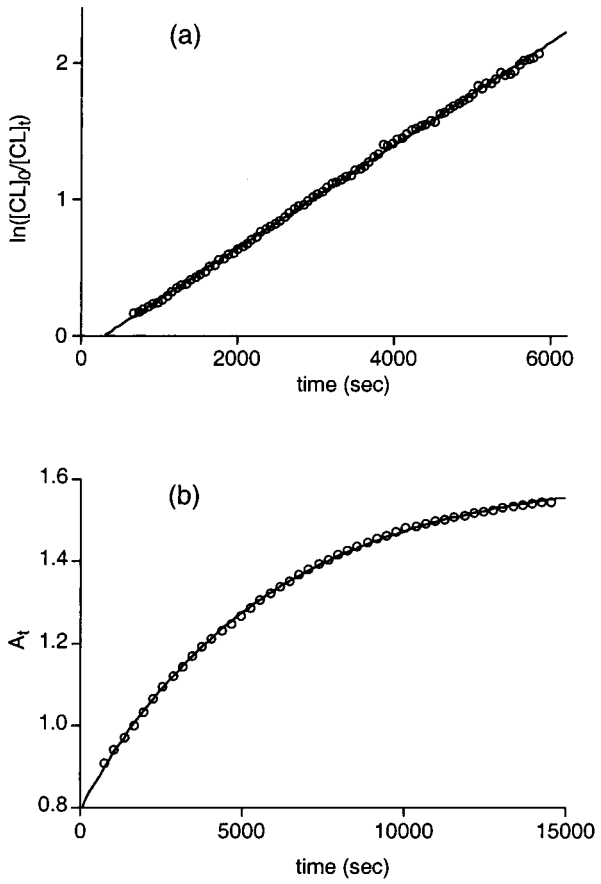

Figure 5. (a) Representative plot of $\ln([Cl]_0/[CL]_t)$ vs time for the polymerization of CL by $Fe_2(OCHPh_2)_6$, showing every second data point acquired with NMR spectroscopy. Conditions: $[CL]_0 = 1.0$ M, $[CL]_0/[Fe]_0 = 550$, d_8-toluene, 25 °C. The slope of the line fit to the data yields $k_{app} = 3.8 \pm 0.2 \times 10^{-4}$ s^{-1}. (b) Representative plot of absorbance of the principle component in FTIR spectra associated with PCL (A_t) vs time for the polymerization of CL by $L_2FeOCHPh_2$, showing every fifth data point. Conditions: $[CL]_0 = 1.0$ M, $[CL]_0/[Fe]_0 = 200$, toluene, 25 °C. The line represents a fit to eq 1, yielding $k_{app} = 1.8 \pm 0.1 \times 10^{-4}$ s^{-1}, $A_0 = 0.80$, $A_\infty = 1.62$.

lently, by fitting the FTIR principle component absorbance data to the equation:

$$A_t = (A_0 - A_\infty)e^{-kt} + A_\infty \qquad (1)$$

where A_t is the absorbance of the PCL component at time t, A_0 is the initial absorbance, and A_∞ is the absorbance at infinite time (Figure 5b). A complete listing of measured k_{app} values is provided in Table S1.

While CL polymerization rates with both catalysts proceeded with the same first-order dependency on [CL], significant differences were observed for their dependencies on the concentration of the catalyst. For $Fe_2(OCHPh_2)_6$, a plot of k_{app} versus $[Fe_2(OCHPh_2)_6]_0$ is linear (Figure 6a), suggesting that the reaction rate is first order in catalyst. However, the *x*-intercept is nonzero, which indicates that there is a threshold catalyst concentration below which no polymerization occurs ($7 \pm 1 \times 10^{-4}$ M). The presence of a constant small amount of an impurity in the monomer or solvent (both present in large excess relative to the catalyst) that quenches a constant amount of the catalyst is consistent with this result. Accordingly, a plot

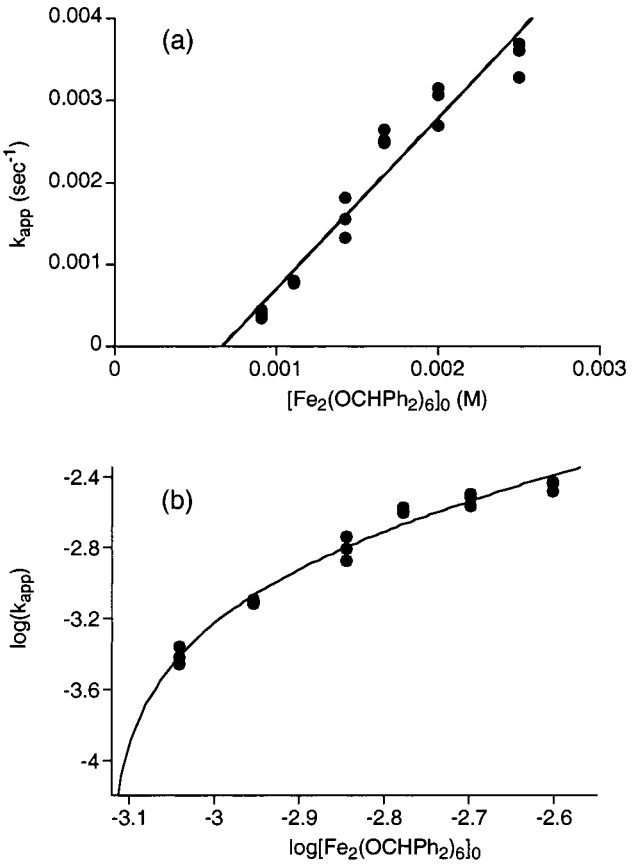

Figure 6. (a) Plot of k_{app} vs $[Fe_2(OCHPh_2)_6]_0$, fit to a straight line with an *x*-intercept $= 7 \pm 1 \times 10^{-4}$ M. (b) Plot of $\log(k_{app})$ vs $\log[Fe_2(OCHPh_2)_6]_0$, with the line representing the fit to eq 2, yielding $k_{prop} = 2.3 \pm 0.1$ M^{-1} s^{-1} and $[I] = 7.4 \pm 0.2 \times 10^{-4}$ M.

of $\log(k_{app})$ versus $\log[Fe_2(OCHPh_2)_6]_0$ should fit to the expression:

$$\log(k_{app}) = \log\{k_{prop}([Fe_2(OCHPh_2)_6]_0 - [I])\} \qquad (2)$$

where I = impurity. The fit to this expression is indeed reasonable (Figure 6b), and yields $k_{prop} = 2.3 \pm 0.1$ M^{-1} s^{-1} and $[I] = 7.4 \pm 0.2 \times 10^{-4}$ M. The latter value agrees well with the *x*-intercept in Figure 6a. Thus, the experimentally determined rate law for CL polymerization by $Fe_2(OCHPh_2)_6$ corresponds to the equation:

$$R_p = -d[CL]/dt = k_{prop}[CL]([Fe_2(OCHPh_2)_6] - [I]) \qquad (3)$$

In contrast, for CL polymerization by $L_2FeOCHPh_2$, a plot of k_{app} versus $[L_2FeOCHPh_2]_0$ (Figure 7a) is decidedly nonlinear, arguing against a first-order dependence on catalyst concentration. A plot of $\log(k_{app})$ versus $\log[L_2FeOCHPh_2]_0$ (Figure 7b) was fit to a straight line of slope $= 0.55 \pm 0.02$, meaning that the order in catalyst is approximately one-half. Thus, the resulting rate law for CL polymerization by $L_2FeOCHPh_2$ is of the form shown in eq 4, where $k' \neq k_{prop}$, as described in more detail below. The line drawn in Figure 7a is a fit to this equation.

$$R_p = -d[CL]/dt = k'[CL][L_2FeOCHPh_2]^{1/2} \qquad (4)$$

Discussion

The deliberate creation of new and versatile catalysts for the polymerization and copolymerization of cyclic esters requires

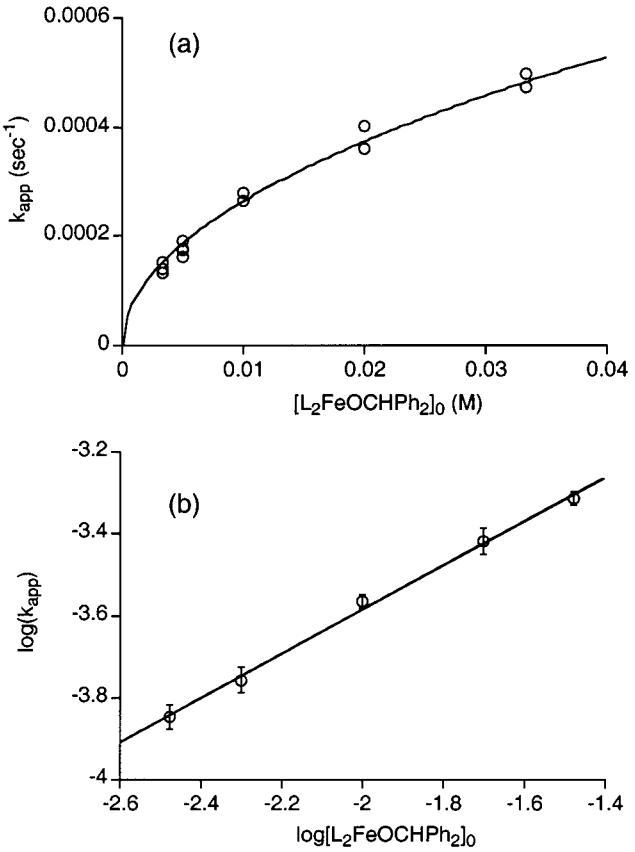

Figure 7. (a) Plot of k_{app} vs $[L_2Fe(OCHPh_2)]_0$, with the line representing a fit to eq 4. (b) Plot of log(k_{app}) (average values) vs log$[L_2Fe(OCHPh_2)]_0$, fit to a straight line with slope = 0.55 ± 0.02.

an understanding of mechanistic similarities and differences among working systems that incorporate related and structurally well-defined precatalyst structures. Through such comparisons, specific influences of catalyst topology on polymerization kinetics and polymer structure may be elucidated, ultimately enabling performance improvements to be implemented through logical catalyst design. In this work, we focused on drawing mechanistic comparisons between representatives of the two general classes of metal complexes that have found extensive use in cyclic ester polymerizations:[1] multimetal−multialkoxide clusters and so-called "single site" mononuclear species with single alkoxide initiators and sterically encumbering supporting ligands. While high activity has been associated with catalysts of the former type, the presence of multiple initiating sites and rapid equilibria among cluster aggregates and/or lower nuclearity fragments may complicate mechanistic analysis. Single site catalysts have been targeted partly in order to obviate these difficulties. We chose to focus specifically on iron(III) catalysts because of the nontoxic nature of this ion that will be incorporated into the polymer product of potential utility in biomedical applications, its ready availability, and the need for improvements in polymerization behavior seen in previously reported iron-based systems.[11] Our discovery[10] of rapid and controlled polymerization of LA by the novel complexes $Fe_5O(OEt)_{13}$ and $Fe_2(OCMe_2Ph)_6$ provided impetus for the work described herein, in which we synthesized and structurally characterized a new set of iron−alkoxide complexes, including mono- and dinuclear species with identical alkoxide initiators, and directly compared their polymerization behavior.

While homoleptic iron(III)−alkoxides have been characterized in solution,[25] we are aware of only one that had been structurally characterized by X-ray diffraction prior to our work, $Li[Fe(OCH(tBu)_2)_4]$.[26] Attempts to isolate "$Fe(OEt)_3$" or related materials have only led to mixed oxide−ethoxide clusters.[10,18,27] We found that reaction of thallium salts of hindered alkoxides with anhydrous $FeCl_3$ smoothly generated the homoleptic complexes $Fe_2(OR)_6$ (R = CMe_2Ph or $CHPh_2$). To prepare single-site analogues of these compounds for comparative mechanistic studies, we chose to use amidinate supporting ligands because of their well-known utility in coordination chemistry,[13] as well as our own findings of their suitability for generating yttrium[28] and tin[29] alkoxide complexes that polymerize LA. A few reports of iron(III)−amidinate complexes have appeared,[15,30−32] and reaction of one of these, L_2FeCl,[15] with thallium alkoxides provided the complexes L_2FeOR (R = Et or $CHPh_2$). Definitive identification of the mono- and diiron alkoxide complexes was accomplished through X-ray crystallography.

We then compared the behavior of $Fe_2(OCHPh_2)_6$ and $L_2FeOCHPh_2$ in polymerizations of LA and CL. While both complexes were effective catalysts, the combined data indicate that the diiron compound generally exhibits a higher degree of polymerization control, particularly for CL. This conclusion is supported by good fits of M_n vs conversion data to a straight line (Figure 3), narrow molecular weight distributions (Table 3), and the ability to prepare a PCL/PLA block copolymer via sequential monomer addition with $Fe_2(OCHPh_2)_6$ (Figure S2). The initiation efficiency as measured by chain lengths in polymerizations carried out at low $[CL]_0/[Fe]_0$ ratios was also greater for the dinuclear catalyst, with approximately every alkoxide in $Fe_2(OCHPh_2)_6$ acting to initiate a growing PCL chain versus only half of the alkoxides being active in the reactions catalyzed by $L_2FeOCHPh_2$. Poorer behavior was observed for both catalysts in polymerizations of LA, as shown by lower levels of molecular weight control (Figure S1), higher PDI values at high conversions, and poorer reproducibility between runs (Table 4). Overall, the LA polymerization behavior of $Fe_2(OCHPh_2)_6$ is superior to that of $L_2FeOCHPh_2$ and is similar to that reported previously for the analogous complex $Fe_2(OCMe_2Ph)_6$, but is inferior to that of $Fe_5(O)(OEt)_{13}$, which displayed better molecular weight control and gave polymers with narrower molecular weight distributions (PDI = 1.11−1.28).[10] Evidently, the amidinate ligands have a detrimental effect on polymerization initiation and propagation by an iron−alkoxide unit, but the underlying reasons for this effect, as well as the other differences among the catalysts studied so far, are unclear.

Kinetic studies were performed to better understand the differences in polymerization reactivity between $Fe_2(OCHPh_2)_6$ and $L_2FeOCHPh_2$, as well as to provide fundamental mechanistic information. These studies focused on the polymerization of CL because of the generally better catalytic behavior with

(25) Bradley, D. C.; Mehrotra, R. C.; Gaur, D. P. *Metal Alkoxides*; Academic Press: London, New York, 1978; pp 87−88.
(26) Bochmann, M.; Wilkinson, G.; Young, G. B.; Hursthouse, M. B.; Malik, K. M. A. *J. Chem. Soc., Dalton Trans.* **1980**, 1863−1871.
(27) Hegetschweiler, K.; Schmalle, H. W.; Streit, H. M.; Gramlicj, V.; Hund, H.-U.; Erni, I. *Inorg. Chem.* **1992**, *31*, 1299−1302.
(28) Aubrecht, K. B.; Chang, K.; Hillmyer, M. A.; Tolman, W. B. *J. Polym. Sci. Part A, Polym. Chem.* **2001**, *39*, 284−293.
(29) Aubrecht, K. B.; Hillmyer, M. A.; Tolman, W. B. *Macromolecules* **2002**, *35*, 644−650.
(30) Clark, J. A.; Kilner, M.; Pietrzykowski, A. *Inorg. Chim. Acta* **1984**, *82*, 85−92.

this monomer, as well as for reasons of convenience. Analysis of the kinetic data led to the experimentally determined rate laws shown as eqs 3 and 4. A first order dependence of the rate of polymerization on [CL] was observed for both catalysts, but the dependence on catalyst concentration differed significantly in a manner that connoted unanticipated mechanistic disparities. For $Fe_2(OCHPh_2)_6$, a first-order dependence on the complex was observed (eq 3), but the nonzero intercept of the k_{app} vs $[Fe_2(OCHPh_2)_6]$ plot indicated that a certain percentage of the catalyst was quenched in every run, presumably by an impurity (I) present in the solvent or monomer. This interpretation was corroborated by the good fit of the data in Figure 6 to eq 3 (or its logarithmic form) for $k_{prop} = 2.3 \pm 0.1\ M^{-1}\ s^{-1}$ and $[I] = 7 \pm 1 \times 10^{-4}$ M. Note that even though this amount of quenching impurity corresponds to less than 0.1% of the initial CL concentration (1.0 M) and thus is difficult to detect or remove, it is sufficient to perturb the observed rate significantly when low concentrations of catalyst are used.[33] Consistent with the implied sensitivity of $Fe_2(OCHPh_2)_6$ to impurities, exposure of solutions of this complex to air and/or water resulted in rapid loss of catalytic activity.

The apparent reaction rates for polymerizations of CL by the mononuclear complex, $L_2FeOCHPh_2$, are over an order of magnitude slower relative to the dinuclear complex at equivalent concentrations of iron.[34] In contrast to the kinetic order (x) of one found for $Fe_2(OCHPh_2)_6$, the x value for $[L_2FeOCHPh_2]$ was found to be approximately one-half (eq 4). Such nonintegral x values have been noted previously for cyclic ester polymerizations and have been interpreted to arise from aggregation of active polymer chains, with propagation of the aggregated species being either slower ($x < 1$) or faster ($x > 1$) than the nonaggregated form.[7,8,21,29,35] According to one model of such a situation potentially applicable to our finding of $x \approx 1/2$, a single aggregate of polymer chains equilibrates with nonaggregated polymer chains, with the assumption that polymerization only occurs from the latter.[35] This is shown in eqs 5 and 6, where P_n is an active polymer chain of degree of polymerization n, $(P_n)_m$ is the aggregate, m is the degree of aggregation, K_{da} is the deaggregation equilibrium constant, and k_{prop} is the intrinsic rate constant of propagation. An expression for k_{app} can be derived from this scheme (eq 7), with the assumption that K_{da} is small (i.e., that essentially all polymer chains are aggregated). According to the logarithmic form of eq 7, the slope of the plot of $\log(k_{app})$ versus $\log[L_2FeOCHPh_2]_0$ is the inverse of the degree of aggregation, m. Thus, the slope of 0.55 in Figure 7b yields a degree of aggregation $m = 2$.

$$(P_n)_m \overset{K_{da}}{\rightleftharpoons} mP_n \tag{5}$$

$$P_n + CL \overset{k_{prop}}{\rightleftharpoons} P_{n+1} \tag{6}$$

$$k_{app} = \frac{k_{prop} K_{da}^{1/m}}{m^{1/m}} [Fe]_0^{1/m} \tag{7}$$

$$k_{app}^{1-m} = \frac{-m k_{prop}^{1-m}}{K_{da}} + k_{prop} k_{app}^{-m} [Fe]_0 \tag{8}$$

While the analysis presented above explains the observed kinetics, it does not allow the determination of K_{da} and k_{prop}. A related expression, which has been derived previously, can be used to extract these parameters (eq 8).[35] Again, this model assumes that polymerization occurs only from nonaggregated chains and that they are in equilibrium with inactive aggregates of a single size, but it makes no assumption as to the magnitude of K_{da}. According to eq 8, a plot of $(k_{app})^{1-m}$ versus $(k_{app})^{-m}[L_2FeOCHPh_2]_0$ has slope k_{prop}, and K_{da} can be obtained from the intercept.[36] The value of m is limited to integer values, and the above analysis suggests that $m = 2$. Thus, a plot of $(k_{app})^{-1}$ versus $(k_{app})^{-2}[L_2FeOCHPh_2]_0$ (Figure S4) yields $k_{prop} = 0.06 \pm 0.02\ M^{-1}\ s^{-1}$ and $K_{da} = 9 \pm 7 \times 10^{-3}$ M, although the linear fit is poor. A better linear fit results when $m = 3$ is used, yielding $k_{prop} = 0.046 \pm 0.003\ M^{-1}\ s^{-1}$ and $K_{da} = 1.7 \pm 0.6 \times 10^{-4}\ M^2$ (Figure S5). However, implicit to this analysis is an improvement of fit as larger m values are used, as well as potentially simplistic assumptions that all aggregates are of a single size and that all aggregates are completely inactive for polymerization. These caveats reflect possible deficiencies in the overall model and suggest significant uncertainty in the actual m value. Nevertheless, the dependence of k_{prop} on m is relatively minor, lending confidence in a rough value for $k_{prop} \approx 0.05 \pm 0.02\ M^{-1}\ s^{-1}$.

The finding that the diiron catalyst with six initiating alkoxides displays simpler kinetics (first order in [catalyst]) than the single site monoiron−monoalkoxide catalyst (half-order dependence) runs counter to the intuitive expectation of the opposite (more complicated kinetics for the cluster with multiple initiators). Aggregation of the CL polymerizing species appears to be more kinetically important for the mononuclear complex,[37] but assessing the underlying reason for this is difficult in the absence of any knowledge of the structure(s) of the aggregate(s). In any case, by comparing the k_{prop} values for CL polymerization by $Fe_2(OCHPh_2)_6$ and $L_2FeOCHPh_2$, we may obtain direct insight into their relative polymerization efficiencies irrespective of their surprising mechanistic disparities. The value for the dinuclear complex ($2.3\ M^{-1}\ s^{-1}$) is ~50 times larger than that for the mononuclear compound ($0.05\ M^{-1}\ s^{-1}$). Within a broader context, the propagation rate constant for $Fe_2(OCHPh_2)_6$ is slightly larger than that of a yttrium alkoxide prepared in situ from the reaction of a yttrium aryloxide and 2-propanol ($k_{prop} = 1.65\ M^{-1}\ s^{-1}$, 22 °C, CH_2Cl_2), apparently the fastest reported CL polymerization catalyst.[38] In contrast, the k_{prop} for $L_2FeOCHPh_2$ is comparable to that of dialkylaluminum alkoxides ($k_{prop} = 0.04\ M^{-1}\ s^{-1}$, 25 °C, THF), complexes that are considered to be among the slowest in cyclic ester polymerizations.[35] The slow propagation by $L_2FeOCHPh_2$ (as well as its poorer initiation efficiency) may be rationalized by

(31) Cotton, F. A.; Daniels, L. M.; Maloney, D. J.; Murillo, C. A. *Inorg. Chim. Acta* **1996**, *242*, 31−42.
(32) Cotton, F. A.; Daniels, L. M.; Maloney, D. J.; Murillo, C. A. *Inorg. Chim. Acta* **1996**, *252*, 293−298.
(33) Note that the presence of such an impurity results in a distortion of the log(k) vs log[complex] plot, and the resulting curvature in such a plot may be misinterpreted as being due to multiple linear segments with divergent orders in [complex].
(34) For example, at the same concentrations of iron atoms $[Fe]_0 = 5.0$ mM at 25 °C: $k_{app}(Fe_2(OCHPh_2)_6) = 3.5 \pm 0.2 \times 10^{-3}\ s^{-1}$ and $k_{app}(L_2FeOCHPh_2) = 1.8 \pm 0.1 \times 10^{-4}\ s^{-1}$.
(35) Duda, A.; Penczek, S. *Makromol. Chem., Macromol. Symp.* **1991**, *47*, 127−140.
(36) Accordingly, k' in eq 4 equals $k_{prop}K_{da}^{1/m}/(m^{1/m})$.
(37) We cannot rule out the possibility that aggregation may become important for polymerizations catalyzed by the diiron complex at higher catalyst concentrations than those used in our studies.
(38) Stevels, W. M.; Ankoné, M. J. K.; Dijkstra, P. J.; Feijen, J. *Macromolecules* **1996**, *29*, 8296−8303.

invoking steric inhibition of monomer binding and/or ring opening by the bulky supporting amidinate ligands. Accordingly, the absence of such ligands in $Fe_2(OCHPh_2)_6$ would rationalize its faster propagation rate.

Conclusion

We have prepared and characterized several new iron(III)−alkoxide complexes, including amidinate-supported single site and homoleptic dinuclear complexes that incorporate the same alkoxide (Ph_2HCO^-), and have compared their reactivity in cyclic ester polymerizations. While both complexes comprising Ph_2HCO^- are effective CL and LA polymerization catalysts, the mononuclear complex shows poorer polymerization behavior. Kinetic investigations revealed that for the polymerization of CL by the dinuclear complex the reaction is first order in both monomer and the diiron complex when taking into account a low-level impurity that deactivates the catalyst. Polymerization of CL by the mononuclear complex displayed kinetics with a similar first-order dependence on [CL], but a dependence on the $[L_2FeOCHPh_2]$ of approximately one-half. This fractional dependence was interpreted by using a model of active chain aggregation, enabling a comparison of k_{prop} values for the mono- and dinuclear systems that revealed ∼50-fold propagation rate enhancement for the latter.

The results reported herein thus present a conundrum. To access single site catalysts that would be expected to exhibit simpler kinetic behavior in cyclic ester polymerizations, sterically hindered ligands that inhibit formation of dimeric (or higher nuclearity) species are required. However, such supporting ligands can drastically slow polymer propagation, and in a counterintuitive fashion, may actually induce aggregation of growing polymer chains, thus complicating the polymerization kinetics and potentially affecting polymer structural features. A more complete understanding of the nature of the reactive species in cyclic ester polymerizations is needed in order to understand these intriguing structure/reactivity relationships and to implement new strategies for catalyst design.

Experimental Section

General Procedures. All air-sensitive reactions were performed in a MBraun glovebox under a N_2 atmosphere or with standard Schlenk techniques. *N*,*N*,*N*′*N*′-Tetramethylethylenediamine (TMEDA), tetrahydrofuran (THF), pentane, and hexamethyldisiloxane (HMDSO) were distilled from Na/benzophenone. Toluene was distilled from sodium. Benzonitrile and $NH(SiMe_3)_2$ were distilled from 3 Å molecular sieves. D,L-Lactide (Aldrich) was recrystallized from dry toluene, sublimed, dissolved in THF, passed through a plug of activated neutral alumina, and pumped to dryness. ϵ-Caprolactone (Aldrich) was dried over CaH_2 and distilled under vacuum. *n*-BuLi (Acros) was titrated with Ph_2CHCO_2H prior to use.[39] Anhydrous $FeCl_3$ was prepared from $FeCl_3 \cdot 6H_2O$ by the method of So and Boudjouk.[40] $PhC(NSiMe_3)_2Li(TMEDA)$ (LLi(TMEDA)) was prepared according to published procedures and the structure was confirmed by ^1H NMR spectroscopy.[41] Benzhydrol (Aldrich) was recrystallized from dry diethyl ether prior to use. TlOEt (Aldrich) was filtered through a plug of Celite prior to use.

Physical Methods. NMR spectra were collected with a Varian VI-300, Varian VXR-300, or Varian VXR-500 spectrometer. Elemental analyses were determined by Oneida Research Services, Whitesboro, NY. IR spectra for characterization were recorded on a Nicolet Avatar 320 FT-IR spectrometer, as Nujol films between NaCl plates. UV−vis specta were recorded on a Hewlett-Packard HP8452A diode array spectrophotometer (190−820 nm scan range). Molecular weights (M_n and M_w) and polydispersities (M_w/M_n) were determined by size exclusion chromatography with respect to polystyrene standards. Samples were analyzed at 40 °C (THF eluent) or 30 °C ($CHCl_3$ or CH_2Cl_2 eluent) with a Waters high performance liquid chromatograph connected to three Jordi Gel DVB columns with pore sizes of 10^4, 10^3, and 500 Å and a Waters 2410 refractive index detector. The solvents were eluted at a flow rate of 1.0 mL/min.

$[Tl(OCHPh_2)]_n$. A solution of TlOEt (2.34 g, 9.38 mmol) in pentane (2 mL) was added to a solution of benzhydrol (1.73 g, 9.39 mmol) in pentane/THF (8 mL/3 mL). A white precipitate formed within 5 min. The reaction mixture was stirred for 16 h, then was filtered off to give $[Tl(OCHPh_2)]_n$ as a colorless crystalline solid (3.30 g, 91%). IR (Nujol, cm^{-1}) 1590, 1487, 1341, 1177, 1079, 1033, 1017, 991, 767, 738, 710, 704, 661, 618, 606; ^1H NMR (500 MHz, d_8-THF) δ 6.44 (d,br, 1H, C*H*), 7.14 (t, 2H, *p*-C*H*), 7.23 (t, 4H, *m*-C*H*), 7.29 (m, 4H, *o*-C*H*). ^{13}C NMR (300 MHz, d_8-THF) δ 81.24 (Ph_2CHO, br), 127.41 (*o*-*C*H), 128.34 (*p*-*C*H, br), 129.32 (*m*-*C*H), 150.28 (*i*-*C*).

$Fe_2(OCHPh_2)_6$. A solution of $[Tl(OCHPh_2)]_n$ (993 mg, 2.56 mmol) in THF (5 mL) was added to a solution of anhydrous $FeCl_3$ (144 mg, 0.891 mmol) in THF (6 mL). A white precipitate formed immediately. The mixture was stirred for 16 h, then filtered through a plug of Celite to remove TlCl, and the resulting yellow solution was reduced to dryness in vacuo. The yellow residue was redissolved in toluene, filtered through Celite, concentrated and stored overnight at −35 °C to give $Fe_2(OCHPh_2)_6$ as a yellow crystalline solid (288 mg, 53%). IR (Nujol, cm^{-1}) 1490, 1332, 1300, 1282, 1260, 1183, 1150, 1082, 1044, 1022, 988, 770, 742, 698, 667, 629. Anal. Calcd for $C_{78}H_{66}O_6Fe_2$: C, 77.36; H, 5.49. Found: C, 77.41; H, 5.38. Crystals suitable for analysis by X-ray diffraction were grown at −35 °C from toluene.

L_2FeCl. This complex has previously been reported in the literature, but was prepared by a different method.[15] A solution of L·Li(TMEDA) (3.24 g, 8.38 mmol) in THF (15 mL) was added to a solution of $FeCl_3$ (0.68 g, 4.21 mmol) in THF (15 mL). The purple solution was stirred at room temperature overnight, and then the solvent was removed in vacuo. Pentane was added and the LiCl was removed by filtration. The filtrate was concentrated in vacuo to about 4 mL and the solution was cooled to −35 °C to produce X-ray quality, dark purple crystals of L_2FeCl (1.61 g, 62%). A unit cell determination by X-ray crystallography of a single crystal of L_2FeCl gave the same unit cell dimensions as those reported previously ($a = 12.097(7)$ Å, $b = 12.776(6)$ Å, $c = 13.174(7)$ Å; $\alpha = 67.35(3)°$, $\beta = 75.56(3)°$, $\gamma = 66.84(3)°$; $V = 1716(1)$ Å^3).[15] IR (Nujol, cm^{-1}) 2360, 1244, 983, 837, 760, 702. Anal. Calcd for $C_{26}H_{46}N_4Si_4ClFe$: C, 50.50; H, 7.50; N, 9.06. Found: C, 50.48; H, 7.33; N, 9.10.

L_2FeOEt. A solution of L_2FeCl (1.19 g, 1.92 mmol) in THF (15 mL) was added to a solution of TlOEt (0.48 g, 1.92 mmol) in THF (15 mL). The resulting terracotta solution was stirred at room temperature overnight. The insoluble TlCl was removed by filtration through Celite and the filtrate was dried in vacuo. The residue was dissolved in pentane and filtered through Celite to remove the remaining insolubles. The filtrate was dried in vacuo, dissolved in 4 mL of a 50/50 HMDSO/pentane mixture, and cooled to −35 °C to produce X-ray quality, dark red crystals of L_2FeOEt (0.69 g, 57%). IR (Nujol, cm^{-1}) 1666, 1260, 1096, 1019, 843, 796; UV−vis (toluene) (λ_{max}, nm (ϵ, M^{-1} cm^{-1})) 395 (2480). Anal. Calcd for $C_{28}H_{51}N_4OSi_4Fe$: C, 53.56; H, 8.19; N, 8.92. Found: C, 53.38; H, 8.02; N, 8.86. Evans method (C_6D_6): $\mu_{eff} = 5.9$ μ_B.

$L_2FeOCHPh_2$. A solution of L_2FeCl (0.72 g, 1.16 mmol) in THF (10 mL) was added to a solution of $[TlOCHPh_2]_n$ (0.45 g, 1.12 mmol) in THF (10 mL). The resulting terracotta solution was stirred at room temperature overnight. The insoluble TlCl was removed by filtration through Celite and the filtrate was dried in vacuo. The residue was

(39) Kofron, W. G.; Baclawski, L. M. *J. Org. Chem.* **1976**, *41*, 1879−1880.
(40) So, J.-H.; Boudjouk, P. *Inorg. Chem.* **1990**, *29*, 1592−1593.
(41) Dick, D. G.; Duchateau, R.; Edema, J. J. H.; Gambarotta, S. *Inorg. Chem.* **1993**, *32*, 1959−1962.

redissolved in pentane and filtered through Celite to remove the remaining insolubles. The filtrate was dried in vacuo, dissolved in 3 mL of pentane, and cooled to −35 °C to produce X-ray quality, dark red crystals of $L_2FeOCHPh_2$ (0.53 g, 59%). IR (Nujol, cm^{-1}) 1666, 1599, 1247, 984, 841, 758, 699; UV−vis (toluene) (λ_{max}, nm (ϵ, M^{-1} cm^{-1})) 395 (2638). Anal. Calcd for $C_{39}H_{57}N_4OSi_4Fe$: C, 61.50; H, 7.50; N, 7.31. Found: C, 61.11; H, 7.61, N, 7.41. Evans method (C_6D_6): $\mu_{eff} = 5.8\ \mu_B$.

X-ray Crystallography. Single crystals of $Fe_2(OCHPh_2)_6$, L_2FeOEt, and $L_2FeOCHPh_2$ were attached to glass fibers and mounted on a Siemens SMART system for data collection at 173(2) K. An initial set of cell constants was calculated from three sets of 20 frames. These initial sets of frames were oriented such that orthogonal wedges of reciprocal space were surveyed; orientation matrices were calculated from 53 to 277 reflections. Final cell constants were collected from a data set that did not exceed 8192 strong reflections from the actual data collection after integration. A randomly oriented region of reciprocal space was surveyed to the extent of 1.3 hemispheres to a resolution of 0.77 Å. Three major swaths of frames were collected in 0.30° steps in ω. Space groups were determined on the basis of systematic absences and intensity statistics.[42] Successful direct-methods solutions were calculated which provided most of the non-hydrogen atoms from the E-maps.[43] Several full-matrix least squares/difference Fourier cycles were performed to locate the remainder of the non-hydrogen atoms. All non-hydrogen atoms were refined with anisotropic displacement parameters (apart from the minor component of the disordered toluene solvate in the structure of $Fe_2(OCHPh_2)_6$). All hydrogen atoms were placed in ideal positions and refined as riding atoms with individual (or group, if appropriate) isotropic displacement parameters. Selected crystallographic data are presented in Table 1 and full data as CIF files for all three structures are included in the Supporting Information.

General Polymerization Procedure. Glassware used for polymerizations was oven or flame-dried, treated with a 1.0 M solution of $(CH_3)_2SiCl_2$, then oven dried for a minimum of 3 h. In the glovebox the treated vial was charged with LA (180 mg, 1.25 mmol) or CL (139 mL, 1.25 mmol) and the appropriate volume of a catalyst solution. The vial was tightly capped, then brought out of the glovebox and stirred immersed in a temperature-controlled bath at 25 or 70 °C. At the appropriate time the mixture was exposed to air and two drops of the reaction mixture was removed and dissolved in $CDCl_3$. The tube was frozen in liquid nitrogen for storage, then thawed prior to analysis by ^{1}H NMR spectroscopy to determine conversion. The remaining reaction mixture was poured into heptane to precipitate the polymer. Excess heptane was decanted off and the polymer mixture was dried at 120 °C prior to SEC analysis.

Kinetics. Data for the polymerization of CL by $Fe_2(OCHPh_2)_6$ were collected by ^{1}H NMR spectroscopy. In the glovebox, a NMR tube was charged with CL and a solution of the catalyst in d_8-toluene, then capped and transferred to an NMR spectrometer for data collection at 25 °C. Conversion was determined by integration of the peaks due to CL and PCL in the region 3.5−4.0 ppm. Three reactions at each catalyst concentration were performed. Apparent rate constants (k_{app}) were extracted by fitting a line to the plot of $\ln\{[CL]_0/[CL]_t\}$ vs time. Data for the polymerization of CL by $L_2FeOCHPh_2$ were collected by in situ monitoring of the changes in the IR spectra using an ASI Applied Systems ReactIR 1000 or ReactIR 4000 spectrometer. In the glovebox, a reaction flask was charged with CL and a solution of the catalyst in toluene, and then the ReactIR probe was attached to the flask via a ground-glass joint. The probe was brought out of the glovebox and attached to the instrument so that the reaction flask was immersed in a temperature-controlled bath set at 25 °C. The program ConcIRT was used to extract profiles and spectra of components that change concentration during the course of a reaction. The spectral window analyzed was 1900−805 cm^{-1}. For each reaction a growth profile due to formation of PCL and a decay profile due to disappearance of CL were observed. Analysis of both PCL growth and CL decay gave very similar results (as did monitoring at a single wavenumber), thus we present only the analysis of PCL growth. Apparent rate constants (k_{app}) were extracted by fitting an exponential curve to the plot of absorbance versus time using eq 1, allowing A_0, A_∞, and k to freely vary. The data were analyzed out to at least four half-lives and at least two reactions were performed at each catalyst concentration. All linear and nonlinear curve fits were performed with KaleidaGraph.

Acknowledgment. We thank the NSF (CHE9975357) for financial support of this work and Dr. Kate Aubrecht for helpful discussions.

Supporting Information Available: Plot of M_n versus conversion for the polymerization of D,L-LA by $Fe_2(OCHPh_2)_6$ and $L_2FeOCHPh_2$ (Figure S1), SEC traces of products of CL/LA copolymerizations (Figure S2), representative stack plot of FTIR spectra (Figure S3), plots of $k_{app}{}^{1-m}$ vs $k_{app}{}^{-m}[Fe]_0$ for varying m values (Figures S4 and S5), and table of k_{app} values (Table S1) (PDF), as well as full X-ray structural information (CIF). This material is available free of charge via the Internet at http://pubs.acs.org.

JA012689T

(42) *SHELXTL-Plus*, V5.1; Siemens Industrial Automation, Inc.: Madison, WI.
(43) *SIR92*: Atomare, A.; Cascarno, G.; Giacovazzo, C.; Gualardi, A. *J. Appl. Crystallogr*. **1993**, *26*, 343.